Fluorescence Studies of the Acetylcholine Receptor: Structure and Dynamics in Membranes and Cells

Francisco J. Barrantes[1]

The nicotinic acetylcholine receptor (AChR) is the archetype member of the superfamily of ligand-gated ion channels that mediate fast intercellular communication in response to endogenous neurotransmitters. Here I review a series of biophysical studies on the AChR protein, with particular focus on the interactions of the macromolecule with its lipid microenvironment. Fluorescence recovery after photobleaching and phosphorescence anisotropy studies of the membrane-embedded AChR have contributed to our understanding of the translational and rotational dynamics of this protein in synthetic lipid bilayers and in the native membrane. Electron spin resonance studies led to the discovery of a lipid fraction in direct contact with the AChR with rotational dynamics 50-fold slower than that of the bulk lipids. This lipid belt region around the AChR molecule has since been intensively studied with the aim to define its possible role in the modulation of receptor function. The polarity and molecular dynamics of solvent dipoles—mainly water—in the vicinity of the lipids in the AChR membrane have been studied exploiting the amphiphilic fluorescent probe Laurdan's exquisite sensitivity to the phase state of the membrane, and Förster-type resonance energy transfer (FRET) was introduced to characterize the receptor-associated lipid microenvironment. FRET was used to discriminate between the bulk lipid and the lipid belt region in the vicinity of the protein. Further refinement of this topographical information was provided by the parallax method using phospholipid spin labels. The AChR–vicinal lipid is in a liquid-ordered phase and exhibits a higher degree of order than the bulk bilayer lipid. Changes in FRET efficiency induced by fatty acids, phospholipid, and cholesterol also led to the identification of discrete sites for these lipids on the AChR protein. I also illustrate the extension of Laurdan fluorescence studies to intact living cells heterologously expressing AChR in a brief section devoted to recent studies using two-photon fluorescence microscopy. The spatial resolution afforded by the two-photon optical sectioning of the cell in combination with the advantageous spectroscopic properties of Laurdan are exploited to obtain information on the physical state of the lipid environment of the membrane. Finally, the application of site-specific labeling and steady-state fluorescence spectroscopy to probe the location of AChR membrane-embedded domains is illustrated. The topography of the pyrene-labeled Cys residues in transmembrane domains αM1, αM4, γM1, and γM4 with respect to the membrane was determined by differential fluorescence quenching with lipid-resident spin-labeled probes. Cys residues were found to lie in a shallow position. For M4 segments, this is compatible with a linear α-helical structure, but not so for M1, for which "classical" models locate Cys residues at the center of the hydrophobic stretch. The transmembrane topography of M1 can be rationalized on the basis of the presence of a substantial amount of nonhelical structure and/or of kinks attributable to the occurrence of the evolutionarily conserved proline residues. The latter is a striking feature of M1 in the AChR and all members of the rapid ligand-gated ion channel superfamily.

KEY WORDS: Cell surface receptors; cholinergic receptor; lipid–protein interactions; Laurdan; annular lipids.

[1] Instituto de Investigaciones Bioquímicas de Bahía Blanca and UNESCO Chair of Biophysics and Molecular Neurobiology, BZW8000 Bahía Blanca, Argentina. Fax: (054) 291 4861200. E-mail: rtfjb1@criba.edu.ar

INTRODUCTION

Membrane proteins constitute roughly one-third of all gene products. Yet only very few high-resolution structures of membrane proteins have been obtained to date, mainly because of the difficulty of obtaining well-ordered three-dimensional crystals. In the absence of detailed information from X-ray or electron crystallographic data, drawing structural–functional correlations of many important membrane proteins has relied on the powerful combination of site-directed mutagenesis and patch-clamp electrophysiology, and various spectroscopic techniques applied to membrane fragments and purified, reconstituted proteins.

Among such important integral membrane proteins is the nicotinic acetylcholine receptor (AChR), one of the best-characterized members of the ligand-gated ion channel superfamily [1], a set of proteins coded by more than a hundred genes so far identified. They exhibit amino acid sequence homology and presumably higher-order structural motifs, though the latter await high-resolution studies for their determination. Within the superfamily, the AChR and the serotonin receptor comprise two families of cation-selective channels, whereas glycine and $GABA_A$ receptors are anion-selective channels. Signal transduction is relatively fast and results from similar mechanistic steps: binding of the neurotransmitter followed by conformational transitions in the receptor proteins that lead to changes in the ionic permeability of the postsynaptic membrane.

In the specific case of the AChR, upon binding, acetylcholine initiates a conformational change in this protein that triggers the transient opening of its intrinsic cation-specific channel across the postsynaptic membrane. At the molecular level, this is accomplished by the concerted action of an array of four different but highly homologous AChR subunits in the stoichiometry $\alpha_2\beta\gamma\delta$ [2–4]. Each AChR subunit contains four putative hydrophobic segments, 20–30 amino acids in length, referred to as M1–M4 and proposed to be membrane-spanning segments. The M2 segment of each subunit is thought to contribute structurally to form the ion channel proper.

On the basis of its hydrophobicity and apparent low degree of sequence conservation, the M4 segment was proposed to be exposed to the bilayer lipid [5,6]. M1 and M3 must have some contact with lipid, since they effectively incorporate membrane-partitioning photoactivatable probes [7–9]. Although the exact topology of these AChR regions relative to the membrane has not yet been determined unambiguously, it is usually accepted that the four hydrophobic segments M1–M4 form the transmembrane (TM) region of the AChR [8,10]. Furthermore, there is still contradictory evidence on their secondary structure. The original postulation of a four-helix bundle with an *all*-helical secondary structure [11] has been challenged by the results of cryoelectron microscopy of frozen AChR tubules [12,13] and computer-aided molecular modeling indicating that the dimensions of the AChR TM region are not compatible with a pentameric four-helix bundle [14]. Site-directed mutagenesis data combined with patch-clamp electrophysiology, and results from photoaffinity labeling with noncompetitive channel blockers, support the notion that the M2 domain lines the walls of the ion channel proper and are indicative of α-helical periodicity in the residues exposed to the lumen of the channel [15]. Recent NMR spectroscopy studies of the δM2 segment [16] indicate that this domain is inserted in the bilayer at an angle of $12°$ relative to the membrane normal, with no kinks, and in a totally α-helical configuration. A synthetic peptide corresponding to the *Torpedo* αM2 segment in chloroform:methanol containing $LiClO_4$ also adopts a totally α-helical configuration [17].

The cryoelectron microscopy studies are further interpreted to indicate that the other putative TM domains (M1, M3, and M4) are relatively featureless, with a large portion of the polypeptide chain in an extended (or unresolved) β-sheet configuration, arranged in the form of a large β-barrel outside the central rim of M2 channel-forming rods [13]. This interpretation is in contrast to the studies using photoactivatable hydrophobic probes, in which the observed periodicity of the lipid-exposed residues in M4 and M3 is consistent with an α-helical pattern [8,9,18] and with deuterium-exchange Fourier transform infrared spectroscopy studies which indicate a predominantly α-helical structure in the AChR TM region [19]. In addition, secondary structure analyses (CD and Fourier transform infrared spectroscopy) of isolated and lipid-reconstituted TM AChR peptides indicate an α-helical structure for M2, M3, and M4 segments [20]. Furthermore, two-dimensional (2D) ^{1}H-NMR spectroscopy of a synthetic peptide corresponding to the αM3 segment of *Torpedo* AChR showed a totally α-helical structure [21], and a recent NMR study of a synthetic γM4 peptide is also compatible with an α-helical secondary structure [22]. In summary, the secondary structure of the AChR TM region is still a matter of debate.

Prior to innervation, the AChR is uniformly distributed on the cell surface. In the course of synaptogenesis, the AChR becomes clustered first in the form of "hot spots," and finally, upon establishment of the neuromuscular junction, receptor molecules adopt the high-density packing characteristic of the adult synapse. It is not known

whether the different organizational modes of the AChR protein are accompanied by large-scale modifications of their lipid environment. We do know, however, that the closely associated lipid belt region surrounding the AChR protein in the electromotor synapse of electrocytes is qualitatively different in terms of molecular mobility [23], and the lipid composition of the synaptic region differs from that of the rest of the membrane in muscle cells [24].

This review deals with biophysical studies focused on some structural and dynamic properties of the AChR molecule, aimed at understanding the relationship between the AChR protein and its membrane environment and, in particular, learning about the topography and dynamics of the AChR and its membrane-associated lipids.

THE CONCEPT OF AChR-ASSOCIATED LIPID

Marsh and Barrantes [23] and Marsh *et al.* [25] obtained one of the first pieces of evidence on the direct interaction between lipid and AChR in its native membrane environment using electron spin resonance (ESR) techniques. This series of studies demonstrated that the protein-associated or "annular" lipids were relatively immobile with respect to the rest of the membrane lipids. Other laboratories [26,27] confirmed these findings and further defined the nature of the protein–lipid interactions using reconstituted systems.

The possible functional implications of the above findings were immediately apparent in early studies [28], demonstrating the need to include cholesterol and certain phospholipids during the receptor purification procedure to preserve the AChR functionality in reconstituted systems. The dissection between phospholipid and sterol requirements was subsequently studied in detail [29–31] and the minimal number of lipids (about 45 molecules) per AChR established in ESR experiments [27,32]. Through this series of experiments it became progressively clear that the AChR–vicinal (annular) lipids were important for the correct functioning of the receptor, but the precise mechanisms by which these annular lipids affected the AChR were not known.

Both sterols and acidic phospholipids were shown to be critical for the proper functioning of the AChR [30,31,33], though others [34] support the view that cholesterol, but not negatively charged phospholipids, is required for AChR activity. In addition, ESR experiments have shown that distinct lipid classes display different affinities for the lipid microenvironment of the AChR [27,35].

DYNAMICS OF AChR AND LIPIDS IN THE MEMBRANE

The highly specialized function of the AChR calls for an organization of the postsynaptic membrane—the natural locus of the AChR—optimally suited to the requirements of signal transduction within the brief operational time scale of the nicotinic synapse. The postsynaptic membrane is, in fact, a closely packed assembly of AChR molecules reaching densities of 10,000–30,000 units μm^{-2}. The clustering of AChRs into discrete supramolecular domains and the maintenance of the large synaptic assembly are two phenomena whose intimate mechanisms have remained elusive for decades. Recent evidence using knockout animals lacking motor nerves or some clustering-inducing factors suggest that AChR are preclustered to the endplate region even in the absence of these two factors. Protein–protein or AChR–lipid interactions are likely to play a role in these preinnervation stages of differentiation of the nicotinic synapse.

One consequence of the organization of AChR into tightly packed clustered assemblies at the synapse is that molecular motions differ from those of nonsynaptic regions of the cell. To what extent are translational and rotational motions hindered at the synapse? Measurements of the dynamics of the AChR protein in synthetic lipid bilayers and in cell membranes are summarized below.

2D Translational Dynamics of the AChR

There is broad agreement that lipid motion in monolayers and bilayers follows in general terms the predictions of the so-called free-area theories, neglecting interactions of the diffusing phospholipid headgroup with the aqueous medium and the fatty acyl chains with the opposing lipid monolayer. Essentially, a lipid molecule undergoes a diffusive step when a free volume (a sort of a "hole") exists adjacent to it, and solvent fluctuations "close" the free volume around the diffusing lipid by jumping into that volume. The free-area theories are used to explain the lateral diffusion coefficient of fluorescent lipid analogues in lipid bilayers. The fluorescent lipid analogue NBD–phosphatidylethanolamine, for instance, exhibits values of D_t, the lateral diffusion coefficient, of 8×10^{-8} cm^2 s^{-1} [30].

When large integral membrane proteins like the AChR—whose dimensions generously exceed those of the surrounding lipids—are reconstituted into artificial bilayers at relatively low protein:lipid ratios, the lateral diffusion of the protein can be approximated by the Saffman and Delbrück [36] formalism. This is based on

the Stokes–Einstein treatment of motion in a solvent medium, in which lateral motion can be envisaged as originating in random collisions of the macromolecule with the solvent molecules and is opposed by frictional forces between the two. The diffusion coefficient, D_t, is given by kT/f, where k is the Boltzmann constant and f is the frictional coefficient. In the case of a spherical molecule of radius r diffusing in a medium of viscosity η, $D_t = kT/6\pi\eta r$ (the Stokes–Einstein equation). Saffman and Delbruck applied this formalism to the case of a cylinder of radius r oriented perpendicular to and diffusing in a thin viscous sheet of viscosity η and thickness h (equal to the height of the embedded cylinder), a treatment that is more relevant to that of a protein transversing a membrane. The diffusion coefficient becomes

$$D_t = (kT/4\pi\eta_m h) \ln(\eta_m h/\eta_w r - 0.577)$$

where η_m is the viscosity of the viscous sheet ("the membrane") and η_w ($\approx 10 \times x^{-2}$ P) is the viscosity of the aqueous medium in which the sheet is immersed. The sheet is treated as a continuum of solvent molecules. The formalism predicts a weak dependence of D on protein radius, a prediction that appears to be followed roughly by the few integral membrane proteins studied to date, including the AChR [30]. It should be noted that the theory finds validity only in the case of very diluted proteins (such as with proteins reconstituted in lipid bilayers).

Various fluorescence recovery after photobleaching (FRAP) studies of adult and embryonic muscle cells have provided useful information on the dynamics of the mobile AChR particles in the membrane and on the fraction of immobile receptors. Most studies concur in that the AChR in the adult synapse and in the patches in developing muscle is translationally immobile, whereas the nonsynaptic areas have AChRs with a higher diffusion coefficient, about 5×10^{-11} cm^2 s^{-1} [37–41]. We studied the lateral diffusion of detergent-solubilized AChR reconstituted in pure dimyristoyl–phosphatidylcholine bilayers and found values of D_t in the range of 10^{-8} cm^2 s^{-1} for both the AChR monomer and dimer in the liquid–crystalline phase and within the 14–37°C range [30]. Additional multiple-component recoveries with D_t values of less than 5×10^{-11} cm^2 s^{-1} were found below the lipid phase transition. Thus in the low concentration limit neither the 9S AChR monomer nor the 13S dimer devoid of rapsyn and other peripheral nonreceptor proteins encounters hindrance to lateral diffusion on the part of the lipid bilayer itself, whereas in native membranes, the densely packed AChR molecules are almost totally anchored and both translational and rotational diffusion are inhibited.

In the plasmalemma of developing rat myotubes, two populations of AChR molecules are observed: a diffusely distributed population having $D_t = 5 \times 10^{-11}$ cm^2 s^{-1} and a localized, patched population with $D_t \approx 10^{-12}$ cm^2 s^{-1} [37]. When blebs are produced in myoblast sarcolemma, D_t is even faster (3×10^{-9} cm^2 s^{-1} [38]). Lack of hindrance to diffusion was also reported for AChR in the plasma membrane of *Xenopus* embryonic myoblasts, where Poo [39] estimated D_t to be 2.6×10^{-9} cm^2 s^{-1}. D in reconstituted membranes is at least 50-fold higher than the highest values found in native membranes. That is, the AChR undergoes essentially free lateral diffusion in a synthetic lipid bilayer, whereas in native membranes or in living cells it exhibits various degrees of hindrance of motion. Reconstituted membranes differ from natural membranes in their lipid composition, concentration of protein, and absence of peripheral proteins. The former factor was not found to influence the lateral diffusion of the AChR at very high lipid: protein ratios. It is likely that the extensive protein–protein interactions occurring both between AChR molecules, on the one hand, and between AChR molecules and other nonreceptor proteins, on the other, are mainly responsible for the relative immobilization of AChR in native membranes, particularly in the synaptic region.

Rotational Dynamics of the AChR

Rotational motion of the AChR protein has been studied by means of ESR and phosphorescence anisotropy techniques. A spectrum of relaxation times is observed with both methods; the rotational correlation time of the monomeric AChR is about 10–25 μs [42], in full agreement with the expected value. Slower relaxation times are probably related to the existence of higher oligomeric AChR species. Early ESR studies [23,25,27,43] showed the rotational immobility of the AChR protein in native AChR-rich membranes purified from fish electric organ. Subsequent reports showed the appearance of rotational motion upon extraction of rapsyn and other nonreceptor peripheral proteins [26]. Extraction of rapsyn gave rise to alterations in AChR packing habits, as judged by electron microscopy [44]. This was interpreted as an increased freedom of motion of the receptor molecules, and it was further proposed that rapsyn plays a role in processes such as synapse formation during ontogenesis, receptor clustering, and stabilization of the adult synapse. Lo *et al.* [45] found enhanced rational freedom of the AChR in membranes depleted of rapsyn by studying the phosphorescence anisotropy of AChR labeled with an erythrosine derivative of α-bungarotoxin. They also reported the restoration of AChR rotational immobility upon reassoci-

ation with the extract containing rapsyn and other peripheral proteins, as confirmed by Rousselet *et al.* [46]. Using the same technique, and eosin derivatives of the α-toxin, we observed a finite rotational correlation time of 12–26 μs associated with the AChR in membranes depleted by rapsyn and other peripheral proteins [42]. The same rotational correlation time was found in dithiothreitol-reduced membranes, though not in native or *N*-ethylmaleimide-alkylated membranes. The experimentally observed relaxation time agreed with that expected for the 9S AChR monomer of about 250,000 Da. Since the translational motion of the AChR in reconstituted pure lipid bilayers can be practically considered a free, unrestricted lateral diffusion (see above), D_t can be related to the rotational relaxation time by $D_t \approx 4r^2/\phi$.

PHYSICAL STATE OF THE AChR–LIPID INTERFACE

Laurdan Fluorescence Spectroscopy Studies

Several fluorescent probes with valuable spectroscopic properties to study membranes are available to date. Figure 1A shows molecular models of representatives probes currently used in the study of AChR–lipid interactions in our laboratory. One particularly advantageous ligand is the fluorescent probe Laurdan (6-dodecanoyl-2-dimethylamino naphthalene). We have characterized the thermotropic behavior of the so-called generalized polarization (GP [47,48]) of Laurdan in AChR-rich membranes from *Torpedo marmorata* [49,50]. In this series of papers, a still unexploited property of Laurdan, namely, its ability to act as a FRET acceptor of tryptophan emission, was introduced to measure some physical properties of the protein–vicinal lipid. FRET between an AChR-rich membrane protein and Laurdan was observed upon excitation at 290 nm (Fig. 1B).

The physical origin of Laurdan spectral properties resides in its extreme sensitivity to the polarity and to the molecular dynamics of dipoles in its environment due to the effect of dipolar relaxation processes reflected as relatively large spectral shifts [47]. Laurdan molecules surrounded by gel-phase lipids, which provide an environment with a low polarity and high order or "rigidity," undergo a lower relaxation process than those localized in an environment of high polarity and "fluidity," such as a liquid–crystalline phase. Since the main solvent dipoles surrounding Laurdan in the membrane are water molecules, when no relaxation occurs, high GP values result, indicative of a low water content in the hydrophilic/hydrophobic interface region of the membrane.
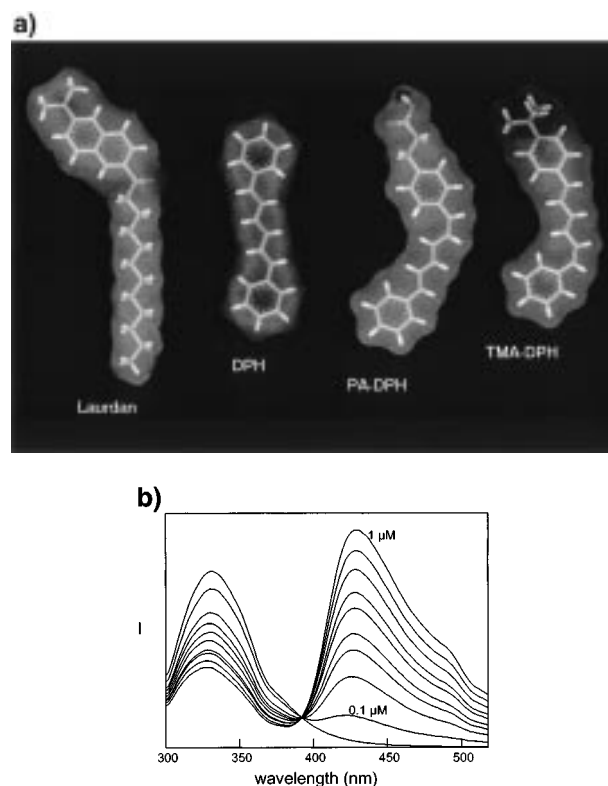

Fig. 1. (A) Examples of fluorescent probes currently used in membrane studies in general and in investigations of AChR–lipid interactions in particular. Molecular models were drawn using the software WebLab Viewer from Molecular Simulations, Inc. (B) Occurrence of Förster's resonant energy transfer (FRET) between a *T. marmorata* AChR-rich membrane and the fluorescent probe Laurdan. Emission spectra were recorded under FRET conditions as a function of the acceptor surface density. A constant molar ratio of AChR protein (donor) in the membrane was maintained, and the Laurdan (acceptor) concentration was varied between 0.1 and 1 μ*M*.

The temperature dependence of Laurdan GP has also contributed to the description and quantification of the phase states of membrane systems. By studying the behavior of Laurdan fluorescence under different excitation/emission wavelengths, it has been possible to characterize qualitatively the phase state of native and artificial membrane systems [48]. Studies of Laurdan GP as a function of temperature (Fig. 2a) and wavelength (Fig. 2b) show that the AChR–lipid interface region, i.e., the AChR–vicinal lipid, differs structurally and dynamically from the bulk bilayer lipid in terms of polarity and molecular motion. Thus, AChR–vicinal lipid exhibits a higher rigidity compared to that in the rest of the membrane bilayer, although a single thermotropic phase with the characteristics of the so-called liquid-ordered phase is present in the AChR postsynaptic membrane [49]. This is not surprising, given the complex lipid composition and
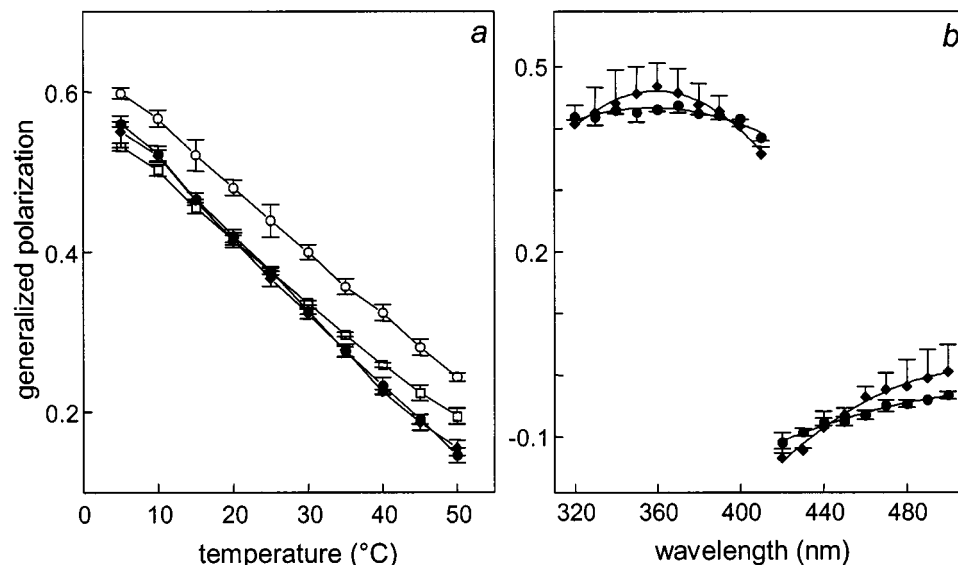
Fig. 2. Laurdan GP (a) as a function of temperature, using direct excitation of the probe at 360 nm (●) or energy transfer (○) from the intrinsic protein fluorescence in native *T. marmorata* AChR-rich membranes (290-nm excitation), and in liposomes prepared from total lipid extracts of these membranes (□, 290 nm; ♦, 360 nm), and (b) as a function of excitation (320 to 410 nm) and emission (420 to 500 nm) wavelengths at 20°C, from *Torpedo* membranes and liposomes prepared from lipids extracted therefrom (●, ♦). Original experimental data from Antollini *et al.* [49].

the high protein:lipid ratio of the native AChR membrane from the electrocyte.

We subsequently extended this type of biophysical studies to living mammalian cells expressing endogenous or heterologous AChR. Interestingly, the differences in physical properties of cell membranes measured by Laurdan GP in a variety of cells, reflecting the molecular dynamics of water molecules, could be correlated with the energetic changes in the AChR ion channel occurring as a function of temperature (Fig. 3), as measured in single-channel recordings [51]. This can be accounted for by the fact that both phenomena report ultimately on the diffusional motion of water molecules. Laurdan expends energy in solvent (water) reorientation, as evidenced in the red shift of its emission spectrum. The decrease in Laurdan GP upon increasing the temperature in turn reflects the increase in water diffusion into the membrane. Water diffusion is facilitated by the increased thermal-induced disorder in the bilayer. The higher AChR channel conductance upon increasing the temperature is a manifestation of the augmented ion and water permeability in the AChR channel or "pore" region as we observed in single-channel recordings with the patch-clamp technique. The study by Zanello *et al.*[51] indicates that AChR channel kinetics depend not only on intrinsic properties of the AChR protein but also on the physical state of the membrane in which the receptor is embedded.

The AChR–lipid microenvironment would thus provide a subtle, "fine-tuning" additional control of channel function.
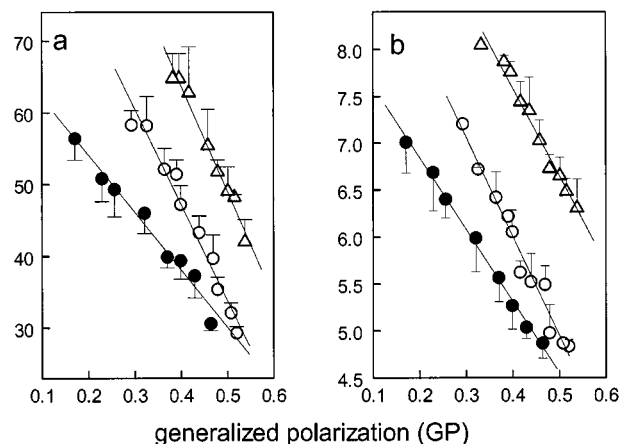

Fig. 3. Relationship between AChR single-channel conductance (a) or channel closing rate, α (b), and Laurdan GP found in three types of cells expressing AChR: CHO-AR-42 (○), BC3H-1 (●), and CHO-K1/A5 (△). Embryonic-type AChR, endogenously expressed in BC3H-1 cells, exhibited a lower Laurdan GP and a lower sensitivity to temperature than AChR (both embryonic and adult type) heterologously expressed in Chinese hamster ovary (CHO) cells, indicating that the energetics of channel closure and the physical properties sensed by Laurdan are determined by the host membrane and are not inherent properties of the AChR protein. From Ref. 51.

Modulation of the Fluidity of the AChR–Lipid Microenvironment

Fong and McNamee [52] showed that reconstituted AChR is sensitive—within a narrow range of values—to the bulk fluidity of the membrane as measured by ion flux experiments. When the fluidity of the host lipid vesicle was varied, as measured by steady-state fluorescence anisotropy of the probe diphenylhexatriene (DPH), ion permeation through the reconstituted AChR was found to occur in either low- or high-fluidity environments [53].

When Laurdan GP was measured in the *Torpedo* native AChR membrane by direct excitation or under FRET conditions in the presence of exogenous lipids, GP and, hence, the "fluidity" and order of the membrane were found to diminish upon the addition of oleic acid and DOPC and not to vary significantly upon the addition of cholesterol hemisuccinate, indicating an increase in the polarity of the single, ordered-liquid lipid phase in the former two cases [50].

Complementary information on the bulk lipid order was obtained from measurements of fluorescence anisotropy of DPH and two of its derivatives. The membrane order diminished in the presence of oleic acid and DOPC. The location of Laurdan was determined using the parallax method of Chattopadhyay and London [54]. Their method is based on the relative position of a fluorescence probe embedded in the membrane and its quenching by probes having nitroxide spin labels at different positions along their acyl chains. The parallax determination is accomplished by pairwise comparison of quenching parameters with different pairwise combinations of the PC analogues 7-SLPC, 10-SLPC, and 12-SLPC. Using this approach, Laurdan was found to lie ~10 Å from the center of the bilayer, i.e., at a depth of ~5 Å from the lipid–water interface [50]. In previous work from our laboratory a minimum donor–acceptor distance of 14 ± 1 Å was calculated for the Laurdan–AChR pair in the *T. marmorata* native membrane [49], in agreement with the overall dimensions of the AChR and its transmembrane region in particular (see Ref. 1).

More recently, we studied the effect of free fatty acids on the *T. marmorata* native membrane and found that saturated free fatty acids increase GP, whereas *cis*-unsaturated fatty acids decrease GP. We were further able to classify these effects from "ordering" to "disordering" in the following series: 20:0 > 18:0 > *cis*18:1 ≅ 18:2 ≅ 20:4 ≅ 22:6 > 18:3. Double-bond isomerism could also be distinguished: oleic acid (*cis*18:1) induced a net disordering effect, whereas elaidic acid (*trans* 18:1) produced no changes in GP (Antollini and Barrantes, unpublished).

LIPID SITES AT THE LIPID–AChR INTERFACE

Various lipids such as fatty acids [55–57], phospholipids containing short-chain fatty acids [58], cholesterol, and steroids [59–61] have been shown to exert effects on AChR function. Both oleic acid and dioleylphosphatidylcholine (DOPC) increase the polarity of bulk and lipid-belt regions in the native AChR membrane, whereas cholesterol hemisuccinate does not induce any statistically significant change in GP. Fluorescence quenching with brominated lipids of AChR intrinsic fluorescence in reconstituted bilayers was used to identify two distinct lipid sites at the lipid–AChR interface: annular sites for phospholipids and nonannular sites for cholesterol, both accessible to free fatty acids [62]. Similar results were obtained by using quenching of pyrene-labeled AChR with brominated lipids [63].

A new strategy for determining the topographical distribution of lipids surrounding the AChR protein was introduced by Antollini and Barrantes [50]. The approach consists of measuring the decrease in the energy transfer efficiency (E) between the intrinsic fluorescence of AChR-rich membranes and Laurdan, induced by different lipids. E between AChR (donor) and Laurdan (acceptor) was calculated using Eqs. (1) and (2) below. According to Förster's theory [64], E is given by

$$E = R_0^6/(R_0^6 + r^6) \tag{1}$$

where r is the intermolecular distance and R_0 is a constant parameter for each donor–acceptor pair, defined as the distance at which E is 50%. E can also be calculated as

$$E = 1 - (\phi/\phi_D) \approx 1 - (I/I_D) \tag{2}$$

where ϕ and ϕ_D are the fluorescence quantum yields of donor in the presence and absence of the acceptor, respectively, and I and I_D are the corresponding emission intensities in any given measurement. The displacement of Laurdan molecules from the AChR microenvironment by exogenously added lipids should diminish the efficiency of the FRET process. This model is based on the assumptions that (i) only Laurdan molecules in close contact with the AChR are excited under FRET conditions and (ii) the added lipids partition in the microenvironment of the protein. Key to these interpretations was the finding that Laurdan did not exhibit selectivity for the AChR microenvironment [49]. The maximal decrease in E resulting from the addition of a fatty acid (18:1) amounted to about 60% (Fig. 4a). The addition of either CHS or DOPC produced a diminution in E of 35 or 25%, respectively (Fig. 4a). The sum of the decreases caused by DOPC and CHS equaled that obtained in the presence of 18:1 alone. This suggested the occurrence of different
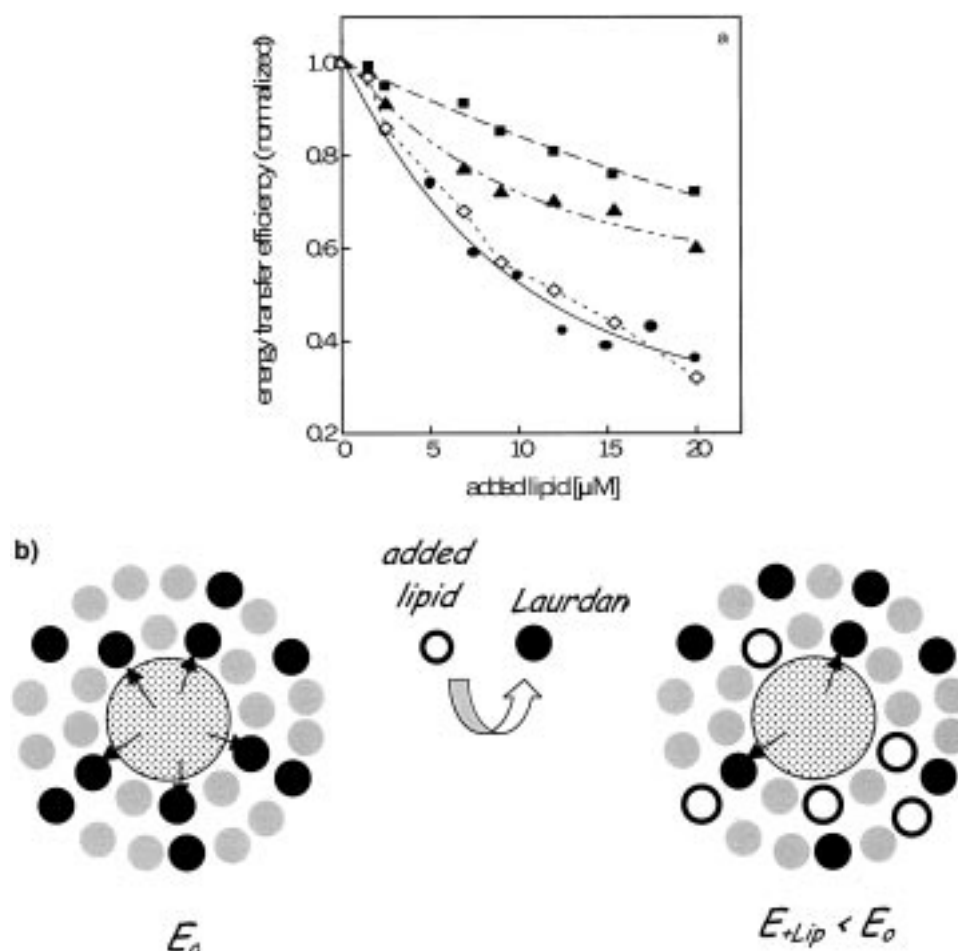
Fig. 4. (a) Displacement of Laurdan by exogenous lipids as measured by changes in FRET efficiency between protein fluorescence and Laurdan emission. The graph shows the normalized FRET efficiency, E, between AChR in native *T. marmorata* membrane and Laurdan upon increasing concentrations of DOPC (■), CHS (○), and oleic acid (●). The curve fitting the ◇ symbols corresponds to the calculated sum of E of DOPC and CHS. All experiments were performed at 20°C. Original experimental data from Ref. 50. (b) Scheme depicting the probable mechanism whereby Laurdan molecules are displaced from the AChR–lipid microenvironment by exogenous lipids. The AChR TM domain is the central shaded circle, the small black circles are Laurdan molecules, and two layers of endogenous lipids are shown as small light-gray circles. E_0 and E_{+Lip} correspond to the efficiency of the energy transfer process (shown by thin black arrows) between the intrinsic membrane fluorescence and Laurdan in the absence and presence of exogenous lipids (shown as open circles), respectively.

sites for DOPC and CHS, both accessible to fatty acid. To corroborate this hypothesis, we saturated one class of sites with either CHS or DOPC and then added a second lipid. In all cases the total effect amounted to ~60%. When oleic acid was added first, an initial reduction of ~60% was obtained, and similar levels of E were attained with subsequent additions of CHS and DOPC. From this series of experiments we reached the conclusion that there are *independent sites* for phospholipid and sterol, both accessible to fatty acid, in the vicinity of the AChR [50]. Access to these sites, and displacement of Laurdan mole-

cules located in the AChR–vicinal lipid belt regions, is shown diagrammatically in Fig. 4b.

The fact that exogenous lipids perturb the physical state of the lipid microenvironment and, more importantly, that *different* lipids interact with *distinct* sites at the lipid–protein interface suggests that (1) there is a direct contact between specific lipids and the AChR, and (2) this contact may be necessary, and probably important, for proper AChR function. Among the key questions remaining to be answered are why cholesterol is needed at the AChR–lipid interface and how fatty acids inhibit

AChR-mediated ionic flux by interacting with "cholesterol sites." Another conclusion from this series of studies is that Laurdan GP and FRET techniques constitute excellent biophysical tools for mapping the topographical distribution of lipophilic compounds such as endogenous lipids and xenobiotics and provide a good approach to learn about the mechanisms by which these compounds act on the AChR–lipid interface, as used recently by Massol *et al.* [65].

LAURDAN GP MEASUREMENT IN LIVING MAMMALIAN CELLS USING TWO-PHOTON EXCITATION

Prior to formation of the synapse, the AChR is uniformly distributed on the cell surface. During synaptogenesis, and before the arrival of the afferent nerve, the AChR at the neuromuscular junction of the muscle cells and electromotor synapses of electrocytes becomes clustered first in the form of "hot spots." This is the "aneural" stage, which depends on activation of a protein kinase termed MuSK. The second phase depends on agrin, a molecule that stabilizes existing clusters and promotes the formation of new ones, while chemical signals originating in the nerve disperse other AChR clusters. Finally, upon establishment of the neuromuscular junction, stable clusters adopt the high-density packing characteristic of the adult synapse.

The advent of new fluorescence microscopies has opened new possibilities for characterizing biophysical properties of membranes *in situ*. We have been exploring the possibilities of some of these techniques using a fibroblast cell line that heterologously expresses adult muscle AChR, thus providing a cellular model of the aneural AChR stages, in an attempt to investigate the possibility that lipid–protein domains contribute to the formation and/or stabilization of AChR clusters. A requisite to such studies is the good spatial resolution of the cell compartments.

When two (or more) infrared photons simultaneously excite a fluorophore rather than a single visible photon, the lower energy per photon of the longer wavelength, as well as the spatial restriction of fluorophore excitation to the focal plane, considerably increases the spatial resolution and reduces the photodamage to the specimen. We used two-photon excitation in an attempt to image Laurdan GP in living cells transfected with AChR. The clonal cell line CHO-K1/A5 was produced in our laboratory by heterologous transfection with the adult muscle AChR subunits [66]. Cells were labeled with Laurdan as in Ref. 67 and examined using excitation

at 795 nm from a mode-locked Ti:sapphire laser [68]. GP images were subsequently calculated from the two-photon raw images. The spatial confinement of the excitation resulting from the use of two photons yielded confocal optical sectioning of the Laurdan fluorescence emission, thus providing excellent resolution of the GP to a thin slice of the cell, as shown in Fig. 5. The topological information yielded by the far-field fluorescence microscopy using multiphoton excitation [67,68] provides a new dimension to understanding the heterogeneous or "patchy" distribution of Laurdan GP and, hence, of the physical state of the lipid milieu of a mammalian cell membrane in which the AChR is embedded.

FLUORESCENCE STUDIES OF THE TOPOGRAPHY OF AChR MEMBRANE-EMBEDDED DOMAINS

The analysis of the topography of AChR membrane-embedded domains has now reached the level of individual peptide segments, as recently investigated using fluorescence quenching techniques with lipid-resident nitroxide spin-labels [69]. Intact *Torpedo californica* AChR protein and transmembrane (TM) peptides prepared by controlled enzymatic digestion were derivatized with *N*-(1-pyrenyl)maleimide (PM), purified, and reconstituted into asolectin liposomes. Fluorescence mapped to proteolytic fragments consistent with PM labeling of cysteine residues in αM1, αM4, γM1, and γM4, as can be observed in a molecular model of the membrane-embedded mass of the receptor (Fig. 6). The labeled cysteine residues are in all cases exposed to the surrounding lipid and located at the "cytoplasmic" end of the AChR TM region, in fact very close to the bilayer–water interface.

The detailed topography of the pyrene labeled Cys residues with respect to the membrane and the apparent affinity for representative lipids were experimentally determined by steady-state differential fluorescence quenching with spin-labeled derivatives of fatty acids, phosphatidylcholine, and the steroids cholestane and androstane. The use of nitroxide spin-label quenching is a well-established method to delineate the relative transbilayer location of the quenched fluorophores, in this case the pyrene-labeled Cys residues, in the membrane. The lipid spin-labels are all lipid-resident molecules embedded at defined depths in the bilayer. Stern–Volmer plots of whole AChR quenching by spin-labeled lipid analogues did not deviate from linearity, and the data were therefore not fitted to a model assuming a fraction of nonaccessible fluorophores [70]. The Stern–Volmer con-
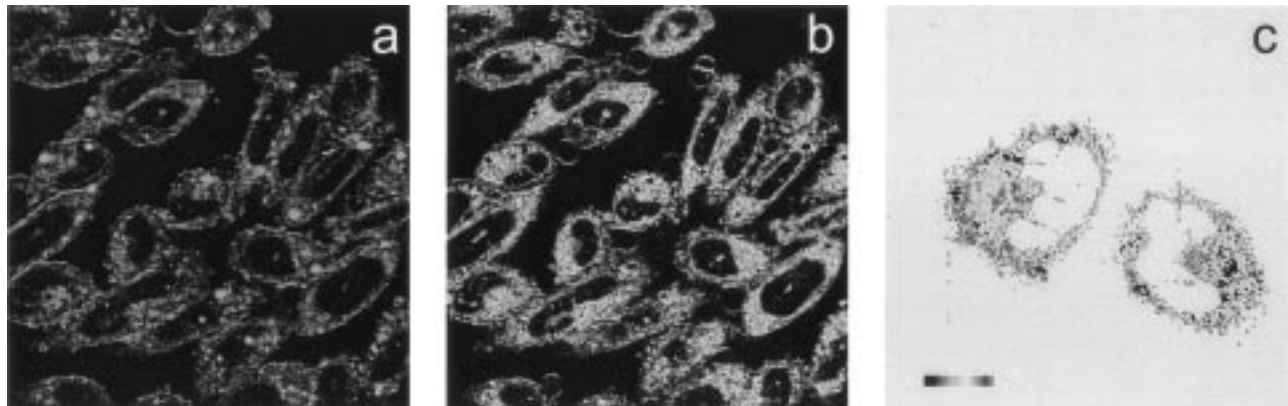
Fig. 5. Two-photon fluorescence microscopy images of Laurdan GP in living mammalian cells. CHO-K1 cells, expressing mouse AChR [66], were stained with 1 μM Laurdan in DMSO in Ham's F-12 medium for 20 min at room temperature and washed for 10 min. Micrographs (512×512 pixels) were digitally recorded in a Leica NT workstation using a Leica 100x 1.4-N.A. oil immersion planapochromatic objective. A 2.0-W average laser power from a Ti:sapphire laser tuned at a wavelength of 795 nm was used. The pulse length of the Gaussian pulse was about 140 fs. Two optical blue and red bandpass filters with a 46-nm bandwidth centered at 446 and 490 nm, respectively, were used to collect raw images like those shown in a and b. Laurdan GP was subsequently calculated offline and images like that shown in c were produced.
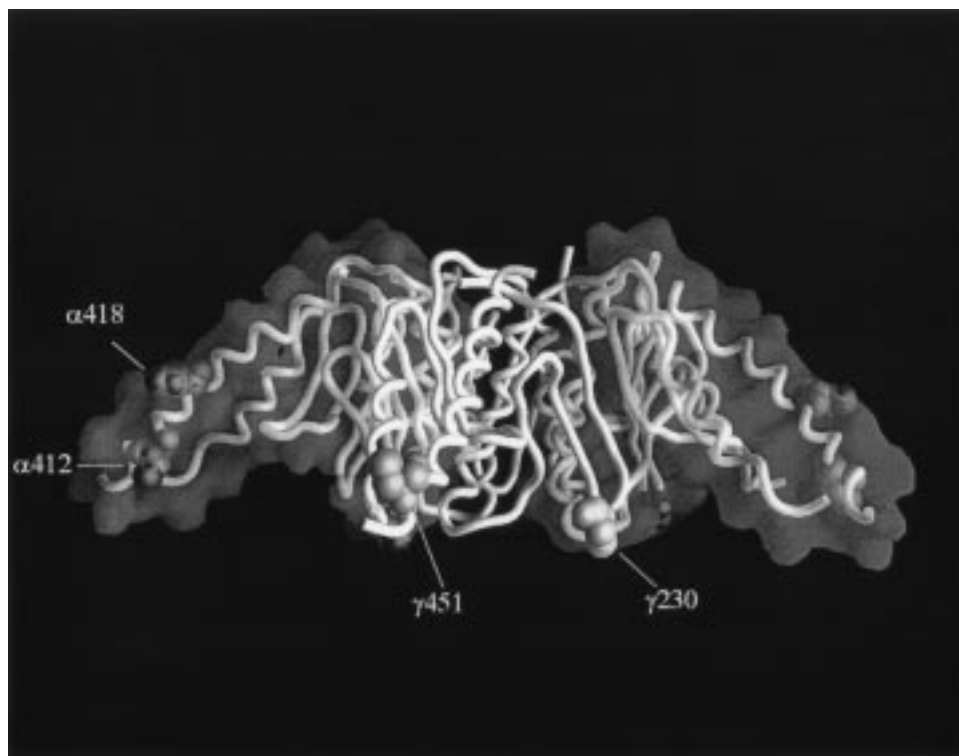

Fig. 6. Molecular model of the AChR transmembrane domain outlining the location of the pyrene-labeled cysteine residues. The model was drawn using the atomic coordinates of Refs. 14 and 71, and the rendering software GRASP. Except for Cys^{418}, which lies in the middle of the $\alpha M4$ segment, all Cys residues are located in a shallow and superficial location in the TM AChR domain. This implies that (i) cysteine residues are closer to the cytoplasmic-facing region of the TM domain, and (ii) they are readily exposed to the surrounding lipid. Individual peptides $\alpha M1$, $\alpha M4$, $\gamma M1$, and $\gamma M4$ were studied in detail (Table I and Ref. 69).

Table I. Stern–Volmer Constants (K_{sv}) for the Quenching of Pyrene-Labeled Transmembrane Fragments and Whole AChR by Spin-Labeled Positional Isomers of Fatty Acids, Phosphatidylcholine, and the Steroids Cholestane and Androstane (from Ref. 69)

K_{sv} (M^{-1})	Whole AChR	α-M1	γ-M1	α-M4	γ-M4
5-SASL	9.87 ± 1.09	6.59 ± 0.48	7.75 ± 0.25	11.44 ± 1.29	12.79 ± 1.45
7-SASL	1.82 ± 0.07	1.46 ± 0.09	2.07 ± 0.14	1.38 ± 0.08	1.83 ± 0.07
12-SASL	1.88 ± 0.04	1.14 ± 0.33	2.09 ± 0.12	1.45 ± 0.02	2.46 ± 0.25
12-PCSL	0.78 ± 0.05	—	—	—	—
CSL	0.21 ± 0.07	—	—	—	0.39 ± 0.06
ASL	3.16 ± 1.00	2.75 ± 0.41	3.43 ± 0.38	2.55 ± 0.27	3.59 ± 0.58

stants K_{SV} are listed in Table I. PM-labeled AChR TM peptides reconstituted into asolectin vesicles were also studied by steady-state fluorescence spectroscopy. 5-SASL and ASL were the most effective quenchers of the pyrenyl fluorescence of whole AChR and derived TM peptides reconstituted into asolectin vesicles (Fig. 7). In the case of spin-labeled stearic acid derivatives, the 5-SASL isomer quenched more effectively than the 7-SASL and the 12-SASL analogues (Table I), indicating a superficial location of the cysteine-bound pyrenes.

Different spin-label lipid analogues exhibit different selectivity for the whole AChR protein and its transmembrane domains. In all cases the quenching studies were compatible with the occurrence of pyrene-labeled Cys residues in a shallow position in the membrane, i.e., closer to the phospholipid polar-head region than to the hydrocarbon core. In the case of γM4, and, by inference, in other M4 segments of the AChR, this is compatible with a linear α-helical structure (Fig. 6). In the case of αM1,

"classical" models locate Cys^{230} at the center of the bilayer in an extended α-helical structure. This is not compatible with the shallow location of pyrene-labeled Cys^{230} emerging from the experimental results [69]. The transmembrane topography of M1 can be explained on the basis of the presence of a substantial amount of nonhelical structure and/or of kinks along M1 (Fig. 6). In a mixed α-helix/β-sheet model of the AChR [71], αM1 was constructed as a three-strand β-sheet interrupted by short loops generated by searching the database of known structures for an appropriate backbone conformation. The proline residues themselves cannot be found within a β-strand, so they were positioned in the loops. The same model can be extended to γM1, having a proline residue (Pro^{229}) immediately adjacent to Cys^{230} and two others (Pro^{222} and Pro^{244}) at the end of the TM region. Thus, the conserved proline residues in the M1 segments of the AChR might introduce "curls" or kinks in a manner analogous to that recently reported for one of the trans-
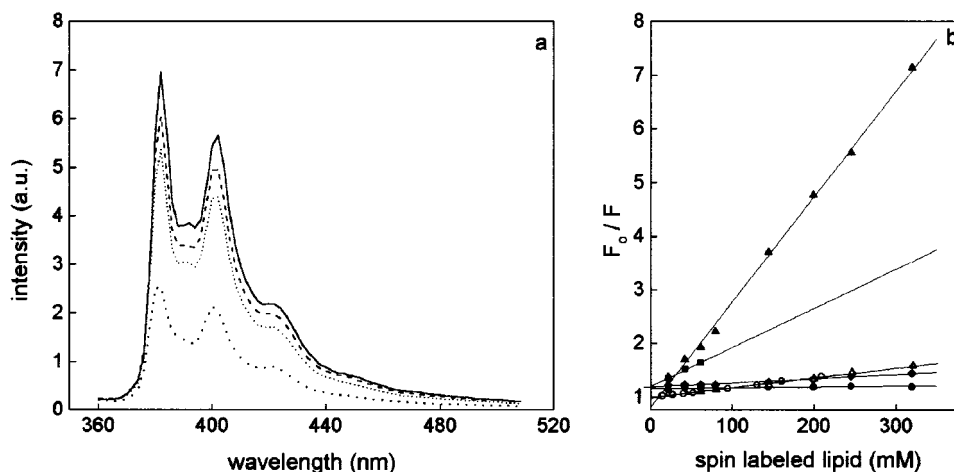

Fig. 7. (a) Fluorescence spectra of pyrene-labeled AChR before (solid line) and after quenching with nitroxide spin-labeled stearic acid analogues (5-SASL, close-dotted line; 7-SASL, spaced-dotted line; 12-SASL, dashed line). (b) F_0 and F correspond to the fluorescence emission of the PM-labeled AChR in the absence and presence of the spin-labeled lipids 5-SASL (▲), 7-SASL (△), 12-SASL (○), ASL (■), CSL (●), and 12-PC-SL (◆), respectively (excitation, 345 nm; emission, 382 nm). From Barrantes *et al.* [69].

membrane segments of a K^+ channel [72]. In the case of the γM1 fragment there appears to be no detailed information on its topography in the membrane as yet, but the occurrence of helix-interrupting proline residues is a striking feature of M1 in the AChR and all members of the rapid ligand-gated ion channel superfamily.

PERSPECTIVES

Only a very limited number of high-resolution structures of membrane proteins have been obtained to date using classical X-ray crystallography methods, mainly because of the difficulty of obtaining large well-ordered three-dimensional crystals. Two-dimensional arrays adequate for electron diffraction techniques have also become available for a few membrane proteins. In the case of the AChR, large tubular structures with helical symmetry can be grown by aging membrane preparations [12,13], but progress has been slow and the resolution so far achieved for the transmembrane region of the protein is much lower than that for the water-exposed part of the molecule (see Ref. 1). In the course of the preparation of this paper the crystal structure of a water-soluble acetylcholine-binding protein from a snail appeared [73]. This remarkable achievement followed the observation that cells of a molluscan cholinergic synapse respond to the natural agonist ACh by releasing a soluble AChR-like protein into the synaptic cleft [74]. This protein captures ACh and thus suppresses synaptic transmission. The release of this decoy glial receptor protein into the synaptic cleft provides a novel mechanism by which glial cells can modulate the efficacy of the complex neuronal chemical communication.

The novel structure determined by crystallographic methods [73] is of great importance to understanding the ligand-recognition (binding) extracellular domain of the highly homologous AChR protein, yet it provides no information whatsoever on the TM domain of the AChR. Structural and dynamic information on the TM region is a needy area and key to understanding membrane proteins such as ligand-gated ion channels, since many physiological and pharmacologically relevant processes affecting these proteins are mediated by, or occur in, the membrane bilayer. It will therefore be necessary to improve currently available structural methods to acquire information in the physiological time window in which synaptic transmission occurs, as is currently the case for some voltage-gated ion channels that can be heterologously expressed in high numbers in oocytes (see, e.g., Ref. 75). Better expression systems will be needed to achieve this goal

in the case of low-expression ligand-gated channels such as the AChR.

Fluorescence is likely to continue playing an invaluable role in these new avenues of research. The availability of new fluorescent probes, and their excitation with near-UV and, in particular, with infrared light, using multiphoton excitation, will result in higher signal-to-noise ratios because of the better separation of excitation and emission. Fluctuation analysis in the form of autocorrelation functions of fluorescence signals—fluorescence correlation microscopy—is already extending the temporal resolution of the classical microscope into that of a rapid kinetics instrument. The possibility of restricting the measurements to femtoliter volumes, even within heterogeneous samples such as cells, adds unique capabilities to the new microscopies. We are witnessing a fast-paced development of fields converging onto the resolution of macromolecular structure and dynamics *in situ*, in nothing less than the living cell: a mind-expanding moment in time. . . .

ACKNOWLEDGMENTS

REFERENCES

1. F. J. Barrantes (Ed.) (1998) *The Nicotinic Acetylcholine Receptor: Current Views and Future Trends*, Springer Verlag, Berlin/Heidelberg, and Landes Georgetown, TX.
2. A. Reynolds and A. Karlin (1978) *Biochemistry* **17**, 2035–2038.
3. J. Lindstrom, J. P. Merlie, and G. Yogeeswaram (1979) *Biochemistry* **18**, 4465–4470.
4. M. A. Raftery, M. W. Hunkapiller, C. D. Strader, and L. E. Hood (1980) *Science* **208**, 1454–1457.
5. J. Giraudat, C. Montecucco, R. Bisson, and J.-P. Changeux (1985) *Biochemistry* **24**, 3121–3127.
6. T. Tobimatsu, Y. Fujita, K. Fukuda, K. Tanaka, Y. Mori, T. Konno, M. Mishina, and S. Numa (1987) *FEBS Lett.* **222**, 56–62.
7. M. P. Blanton and H. H. Wang (1991) *Biochim. Biophys. Acta* **1067**, 1–8.
8. M. P. Blanton and J. B. Cohen (1992) *Biochemistry* **31**, 3738–3750.
9. M. P. Blanton and J. B. Cohen (1994) *Biochemistry* **33**, 2859–2872.
10. R. A. Chavez and Z. W. Hall (1992) *J. Cell Biol.* **116**, 385–393.
11. M. Noda, H. Takahashi, T. Tanabe, M. Toyosato, S. Kikyotani, T. Hirose, M. Asai, H. Takashima, S. Inayama, T. Miyata, and S. Numa (1983) *Nature* **299**, 793–797.

12. N. Unwin (1993) *J. Mol. Biol.* **229**, 1101–1124.

13. N. Unwin (1995) *Nature* **373**, 37–43.

14. M. O. Ortells, G. E. Barrantes, and F. J. Barrantes (1998) in F. J. Barrantes (Ed.), *The Nicotinic Acetylcholine Receptor: Current Views and Future Trends*, Springer Verlag, Berlin/Heidelberg, and Landes, Georgetown, TX, pp. 85–108.

15. J. P. Changeux and S. J. Edelstein (1998) *Neuron* **21**, 959–980.

16. S. J. Opella, F. M. Marassi, J. J. Gesell, A. P. Valente, Y. Kim, M. Oblatt-Montal, and M. Montal (1999) *Nature Struct. Biol.* **6**, 374–379.

17. V. S. Pashkov, I. V. Maslenikov, L. D. Tchikin, R. G. Efremov, V. T. Ivanov, and A. S. Arseniev (1999) *FEBS Lett.* **457**, 117–121.

18. M. P. Blanton, E. A. McCardy, A. Huggins, and D. Parikh (1998) *Biochemistry* **37**, 14545–14555.

19. J. E. Baenziger and N. Méthot (1996) *J. Biol. Chem.* **270**, 29129–29137.

20. J. Corbin, N. Méthot, H. H. Wang, J. E. Baenziger, and M. P. Blanton (1998) *J. Biol. Chem.* **273**, 771–777.

21. A. A. Lugovskoy, I. V. Maslennikov, Y. N. Utkin, V. I., Tsetlin, J. B. Cohen, and A. S. Arseniev (1998) *Eur. J. Biochem.* **255**, 455–461.

22. P. F. Williamson, B. Bonev, F. J. Barrantes, and A. Watts (2000) *Biophys. J.* **78**, 147A.

23. D. Marsh and F. J. Barrantes (1978) *Proc. Natl. Acad. Sci. USA* **75**, 4329–4333.

24. R. J. Bloch and J. S. Morrow (1989) *J. Cell Biol.* **108**, 481–494.

25. D. Marsh, A. Watts, and F. J. Barrantes (1981) *Biochim. Biophys. Acta* **645**, 97–101.

26. A. Rousselet, P. F. Devaux, and K. W. Wirtz (1979) *Biochem. Biophys. Res. Commun.* **90**, 871–877.

27. J. F. Ellena, M. A. Blazing, and M. G. McNamee (1983) *Biochemistry* **22**, 5523–5535.

28. M. Epstein and E. Racker (1978) *J. Biol. Chem.* **253**, 6660–6662.

29. E. L. Ochoa, A. W. Dalziel, and M. G. McNamee (1983) *Biochim. Biophys. Acta* **727**, 151–162.

30. M. Criado, H. Eibl, and F. J. Barrantes (1982) *Biochemistry* **21**, 3622–3629.

31. M. Criado, H. Eibl, and F. J. Barrantes (1984) *J. Biol. Chem.* **259**, 9188–9198.

32. O. T. Jones, J. H. Eubanks, J. P. Earnest, and M. G. McNamee (1988) *Biochemistry* **27**, 3733–3742.

33. T. M. Fong and M. G. McNamee (1986) *Biochemistry* **25**, 830–840.

34. S. E. Rankin, G. H. Addona, M. A. Kloczewiak, B. Bugge, and K. W. Miller (1997) *Biophys. J.* **73**, 2446–2455.

35. M. Dreger, M. Krauss, A. Herrmann, and F. Hucho (1997) *Biochemistry* **36**, 839–847.

36. P. G. Saffman and M. Delbrück (1975) *Proc. Natl. Acad. Sci. USA* **72**, 2035–2038.

37. D. Axelrod, D. E. Koppel, J. Schlessinger, E. Elson, and W. W. Webb (1976) *Biophys. J.* **16**, 1055–1069.

38. D. W. Tank, E.-S. Wu, and W. W. Webb (1982) *J. Cell Biol.* **92**, 207–212.

39. M.-M. Poo (1982) *Nature* **295**, 332–334.

40. D. Axelrod, P. M. Ravdin, and T. R. Podleski (1978) *Biochim. Biophys. Acta* **511**, 23–38.

41. D. Axelrod, A. Wright, W. W. Webb, and A. Horitz (1979) *Biochemistry* **17**, 3604–3609.

42. M. Bartholdi, F. J. Barrantes, and T. M. Jovin (1981) *Eur. J. Biochem.* **120**, 389–387.

43. A. Rousselet and P. F. Devaux (1977) *Biochem. Biophys. Res. Commun.* **78**, 448–454.

44. F. J. Barrantes, D. C. Neugebauer, and H. P. Zingsheim (1980) *FEBS Lett.* **112**, 73–78.

45. M. M. S. Lo, P. B. Garland, J. Lamprecht, and E. A. Barnard (1980) *FEBS Lett.* **111**, 407–412.

46. A. Rousselet, J. Cartaud, and P. F. Devaux (1981) *Biochim. Biophys. Acta* **648**, 169–185.

47. T. Parasassi, G. De Stasio, A. d'Ubaldo, and E. Gratton (1990) *Biophys. J.* **57**, 1179–1186.

48. T. Parasassi, G. De Stasio, G. Ravagnan, R. M. Rusch, and E. Gratton (1991) *Biophys. J.* **60**, 179–189.

49. S. S. Antollini, M. A. Soto, I. Bonini de Romanelli, C. Gutierrez-Merino, P. Sotomayor, and F. J. Barrantes (1996) *Biophys. J.* **70**, 1275–1284.

50. S. S. Antollini and F. J. Barrantes (1998) *Biochemistry* **37**, 16653–16662.

51. L. P. Zanello, E. Aztiria, S. S. Antollini, and F. J. Barrantes (1996) *Biophys. J.* **70**, 2155–2164.

52. T. M. Fong and M. G. McNamee (1987) *Biochemistry* **26**, 3871–3880.

53. C. Sunshine and M. G. McNamee (1994) *Biochim. Biophys. Acta* **1191**, 59–64.

54. A. Chattopadhyay and E. London (1987) *Biochemistry* **26**, 39–45.

55. T. J. Andreasen, D. R. Doerge, and M. G. McNamee (1979) *Arch. Biochem. Biophys.* **194**, 468–480.

56. T. J. Andreasen and M. G. McNamee (1980) *Biochemistry* **19**, 4719–4726.

57. C. B. Bouzat and F. J. Barrantes (1993) *Receptors Channels* **1**, 251–258.

58. M. S. Braun and D. A. Haydon (1991) *Pflugers Arch.* **418**, 62–67.

59. C. B. Bouzat and F. J. Barrantes (1993) *NeuroReport* **4**, 143–146.

60. C. B. Bouzat and F. J. Barrantes (1993) *Mol. Neuropharm.* **3**, 109–116.

61. C. B. Bouzat and F. J. Barrantes (1996) *J. Biol. Chem.* **271**, 25835–25841.

62. O. T. Jones and M. G. McNamee (1988) *Biochemistry* **27**, 2364–2374.

63. V. Narayanaswami and M. G. McNamee (1993) *Biochemistry* **32**, 12420–12427.

64. Förster Th. (1948) *Ann. Phys. (Leipzig)* **2**, 55–75.

65. R. Massol, S. S. Antollini, and F. J. Barrantes (2000) *Neuropharmacology* **39**, 1095–1106.

66. A. M. Roccamo, M. F. Pediconi, E. L. Aztiria, L. Zanello, A. Wolstenholme, and F. J. Barrantes (1999) *Eur. J. Neurosci.* **11**, 1615–1623.

67. T. Parasassi, E. Gratton, W. M. Yu, P. Wilson, and M. Levi (1997) *Biophys. J.* **72**, 2413–2429.

68. S. W. Hell (1997) in J. Lakowicz (Ed.), *Topics in Fluorescence Spectroscopy; Nonlinear and Two-Photon-Induced Fluorescence*, Plenum Press, New York, Vol. 5, pp. 361–426.

69. F. J. Barrantes, S. S. Antollini, M. P. Blanton, and M. Prieto (2000) *J. Biol. Chem.* **275**, 37333–37339.

70. S. S. Lehrer (1971) *Biochemistry* **10**, 3254–3263.

71. M. O. Ortells and G. G. Lunt (1996) *Protein Eng.* **9**, 51–59.

72. D. del Camino, M. Holmgren, Y. Liu, and G. Yellen (2000) *Nature* **403**, 321–325.

73. K. Brejc, W. J. van Dijk, R. V. Klaassen, M. Schuurmans, J. van der Oost, A. B. Smit, and T. K. Sixma (2001) *Nature* **411**, 269–276.

74. A. B. Smit, N. I. Syed, D. Schaap, J. van Minnen, J. Klumpermank, K. S. Kits, H. Lodder, R. C. van der Schors, R. Â. van Elk, B. Sorgedrager, K. Æ. Brejc, T. K. Sixma, and W. P. M. Geraerts (2001) *Nature* **411**, 261–268.

75. A. Cha, G. E. Snyder, P. R. Selvin, and F. Bezanilla (1999) *Nature* **402**, 809–813.